Computers & Fluids 53 (2012) 40–52

Contents lists available at SciVerse ScienceDirect

Computers & Fluids

journal homepage: www.elsevier.com/locate/compfluid

Vortex shedding characteristics of a circular cylinder with an oscillating wake splitter plate

Y. Sudhakar, S. Vengadesan *

Fluid Mechanics Laboratory, Department of Applied Mechanics, Indian Institute of Technology Madras, Chennai 600 036, India

ARTICLE INFO

Article history:
Received 20 December 2010
Received in revised form 3 September 2011
Accepted 10 September 2011
Available online 17 September 2011

Keywords:
Splitter plate
Vortex shedding
Passive flow control
Formation length
Vortex interaction

ABSTRACT

The vortex shedding characteristics and the drag force acting on a circular cylinder, attached with an oscillating splitter plate, are investigated by solving the two-dimensional Navier–Stokes equations. The splitter plate is forced to exhibit harmonic oscillation about its attachment point, and the Reynolds number (*Re*) of the flow is 100. In order to facilitate easy handling of the plate oscillations inside the computational domain, the equations are solved in a Cartesian grid, and the concept of immersed boundary method is used to impose the boundary conditions on the body surface. The characteristic feature of this problem is the complex interaction between the vortices shed from the splitter plate and the cylinder. Three different patterns of vortex shedding are observed in the wake of the circular cylinder depending upon the frequency and amplitude of plate oscillation: normal shedding, chain of vortices and shedding from splitter plate. It is found that the inverse relationship between the vortex formation length and Strouhal number is not applicable when the splitter plate is subjected to oscillation. Additional related interesting fluid dynamics features are also presented.

1. Introduction

Two symmetrically placed attached eddies develop in the rear of the circular cylinder, when Reynolds number, *Re* ($=\rho VD/\mu$) of the flow is very low; where ρ and μ are the density and dynamic viscosity of the fluid respectively, V is the free-stream velocity, and D is the diameter of the cylinder. When *Re* of the flow exceeds 47, instability develops in the flow field which results in unsteady separation of flow from both sides of the cylinder. The vortices, which were attached at low *Re*, start to peel off periodically from the cylinder, and this phenomenon is known as von-Karman vortex shedding. Bluff structures are subjected to vibrations as the vortex shedding induces fluctuating pressure loads on them. These vortex induced vibrations arise in many practical situations such as heat exchanger tube bundles, marine structures, bridges, power transmission lines etc. [1]. Hence, it is mandatory to control the vortex shedding from bluff bodies to prevent the possible structural damage.

Wake splitter plate is used frequently as a passive method to control the vortex shedding. When the length of the splitter plate was only 1D, the vortex shedding was not completely attenuated, but the Strouhal number (*St*) and drag coefficient (C_D) were found to decrease. Experiments conducted by Roshko [2] showed that the inclusion of a splitter plate of 5 diameters long inhibited the vortex shedding and resulted in increased base pressure. Gerrard [3] investigated the frequency of vortex shedding behind a cylinder with attached splitter plates of various lengths up to 2D. His measurements indicated that the *St* was decreased as the length of splitter plate was increased, and the minimum *St* was observed when the length of the plate is approximately equal to *D*. Further increase in the length of splitter plate resulted in the increased *St*. It has been shown that the frequency of vortex shedding was inversely proportional to the formation length of the vortices.

Measurements of pressure distribution around the cylinder, frequency of vortex shedding and flow visualization were performed in the *Re* range $10^4 < Re < 5 \times 10^4$ to study the influence of splitter plate [4]. Splitter plate reduced the drag markedly by stabilizing the separation points and produced a wake narrower than that for a plain cylinder. It raised the base pressure by as much as 50% and affected the *St* to a less degree. Experiments were conducted to assess the influence of the length of splitter plate (L), and it was found that when $L/D = 1$, both C_D and *St* attained a minimal value.

Experiments on flow over a circular cylinder with splitter plate were conducted by Unal and Rockwell [5,6] in the *Re* range of $140 < Re < 1600$. The flow patterns observed were divided into two separate regions: pre-vortex formation regime and post-vortex formation regime. The pre- and post-vortex formation regimes were characterized by the absence and presence of large-scale vortices upstream of the plate's tip respectively. The unsteady pressure forces acting on the plate were found to change drastically when the plate was moved from the one regime to another.

* Corresponding author. Tel.: +91 44 2257 4063; fax: +91 44 2257 4050.
E-mail address: vengades@iitm.ac.in (S. Vengadesan).

0045-7930/$ - see front matter © 2011 Elsevier Ltd. All rights reserved.
doi:10.1016/j.compfluid.2011.09.003

Cimbala and Garg [7] studied the influence of splitter plate on a freely rotatable cylinder, and reported that splitter plate of $L/D < 5$ were not aligned with the free-stream flow. The formation length and the frequency of von Karman vortex shedding were completely different between the rotatable plate and a fixed one when $L/D < 2$. For greater L/D, they behaved in the same way even though the rotatable cylinder-plate combinations were not aligned with the free-stream flow. The inverse relationship between the formation length and the shedding frequency (proposed by Gerrard [3]) was found to be applicable for the rotatable cylinder also.

Nakamura [8] carried out experiments on flow over several bluff body shapes attached with a splitter plate. The *Re* of the experiments ranged from 300 to 5000. When the splitter plate is attached to the bluff body, the vortex shedding characteristics is changed from Karman shedding (which is a double-layer instability) into impinging shear layer instability (which is a single-layer instability). It was reported that *St* based on streamwise distance of the body was only weakly dependent on *Re* and sectional geometry.

The vortex shedding behind a circular cylinder and its control using a splitter plate over the *Re* range of 80–160 were investigated in a numerical study [9]. For $Re \leqslant 100$, the *St* decreased continuously as L/D was increased. For $Re \geqslant 120$, the St reached a local maximum when $L/D = 2$ and decreased when L/D was further increased. It was observed that the interaction between the secondary vortex formed on the plate and the primary vortex from the cylinder was responsible for the increased *St* when $Re \geqslant 120$. Secondary vortices did not form on the plate when $Re \leqslant 100$.

In an another study, the reduction of drag forces and Strouhal number for flow past a circular cylinder with a detached splitter plate were reported over the Reynolds number range of $30 \leqslant Re \leqslant 160$ and $L/D = 1$ [10]. The splitter plate was placed at a distance of G from the base of the cylinder. They found that at optimal location distance of the plate, the C_D was less than the attached plate case. Abrupt change in the nature of the flow and sudden increase in C_D and *St* were found when G/D was increased from 2.6 to 2.7. When $G/D > 2.6$, the splitter plate also shed vortices periodically. The complex interaction between the vortex shedding from the cylinder and splitter plate resulted in increased C_D and *St*.

Flows past a circular cylinder exhibiting forced cross-flow oscillations in a straight channel with an upstream splitter plate were performed at $Re = 100$ by utilizing an unstructured spectral/hp element algorithm based on the ALE formulations [11]. They investigated the flow field for wide range of cylinder oscillation frequencies, including the sub-harmonic, super-harmonic, and primary lock-in regimes. The study revealed a number of interesting phenomena for different cylinder frequency values. It was shown that the use of upstream splitter plate enhanced the mixing characteristics also.

In a water tunnel, flow induced in-line oscillation of a circular cylinder was studied in free-oscillation tests [12]. Two different types of excitation phenomena appeared at approximately half of the resonance velocity. The amplitude of oscillation of the vibrating cylinder increased when the splitter plate was inserted in the wake of the cylinder. It led to the conclusion that the alternate shedding of vortices reduced the amplitude of vibration.

Recently, Shukla et al. [13] reported the influence of a hinged-rigid splitter plate in the wake of a circular cylinder. The hinged-splitter plate did not destroy the communication between the shear layers completely: the pressure difference across the splitter plate resulted in the occurrence of sustained oscillations of the plate. The tip amplitude of the plate reached a maximum value of 0.45D. The oscillation of the splitter plate changed from periodic to aperiodic when L/D was increased beyond 3.

In this numerical study, the vortex shedding characteristics of a circular cylinder attached with an oscillating splitter plate is studied. The splitter plate is forced to exhibit simple harmonic motion. The influence of varying the amplitude and frequency of splitter plate oscillations are reported. This paper is organized as follows. In Section 2, the geometry and the kinematic parameters are explained in-detail. The numerical methodology used to solve the governing equations is presented in Section 3. In Section 4, the shear layer stabilizing effect of attached stationary splitter plate is demonstrated, which is also used as a validation study for our solver. In Section 5, the results of varying the frequency and amplitude of splitter plate on the force coefficients and the flow structures are discussed. Finally, the conclusions drawn from our study are explained in Section 6.

2. Problem definition

In addition to the studies explained in the previous section, many other researchers have conducted experiments on bluff bodies to understand the flow modification due to the attachment of splitter plate. The summary of available literature points out that though the splitter plate is efficient in attenuating the vortex shedding from the bluff body, it requires a very long plate ($L/D = 5$) in order to completely suppress the shedding. The main objective of the study is to investigate whether is it possible to suppress the vortex shedding from the cylinder by attaching an oscillating splitter plate of smaller length. Moreover, though many studies have been performed to study the influence of fixed splitter plate on fixed and oscillating bluff body, the vortex shedding characteristics of a bluff body with an oscillating splitter plate is not yet investigated. To gain further insights into the vortex shedding process of a bluff body, we attach a wake splitter plate to the base of a circular cylinder and oscillate the plate harmonically about the attachment point as shown in Fig. 1. In the experiments of Shukla et al. [13], the splitter plate was hinged to the cylinder, and the plate was free to move depending upon the pressure difference between top and bottom surface of the plate. Given the freedom to move, the plate exhibited periodic oscillations when $L/D \leqslant 3$. However, in present simulations the splitter plate is forced to undergo periodic sinusoidal oscillation.

We present results on the influence of varying the amplitude and frequency of the splitter plate on a circular cylinder by numerically solving the two-dimensional Navier–Stokes equations at $Re = 100$. For a circular cylinder, the three-dimensionality of the flow evolves only at *Re* of 160 [14]. Hence solving the two-dimensional equations will give physically relevant solution for the considered case at $Re = 100$. Moreover, we take length of the splitter plate equal to the diameter of the cylinder ($L/D = 1$). Because it has been shown by the researchers that when $L/D = 1$, the *St* was found to be minimum [3,4]. We varied the amplitude (A) of splitter plate from $0.1D$ to $0.5D$, and the non-dimensional frequency ($f_s = fD/V$, where f is the dimensional frequency of splitter plate and V is the free-stream velocity) is ranged from 0.0825 to 0.5. In

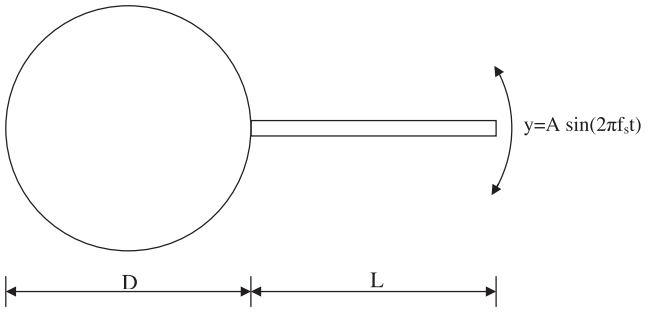

Fig. 1. Geometry and kinematics of wake splitter plate.

the experiments of Shukla et al. [13], the plate moved with the maximum amplitude of 0.45D and the non-dimensionalized natural vortex shedding frequency (St) from circular cylinder was 0.165. Hence, the considered frequency range is well above and below this shedding frequency. The use of periodic function for the splitter plate movement is meaningful because when $L/D \leqslant 3$, the hinged splitter plate exhibited periodic motion [13].

3. Numerical methodology

While using conventional CFD methods, body-fitted grid is generated around the body under consideration, and the governing conservation equations are solved on this grid. If the body immersed in the flow field is moving, as in our case, one way of accommodating the movement of the body is to deform the initial mesh generated. In order to achieve this, a Laplace equation should be solved for obtaining the mesh velocity at every point [11]. Besides in order to avoid problems associated with mesh tangling, a small computational time step should be used in such numerical simulations. The above mentioned difficulties, namely the requirement to solve a Laplace equation and the necessity to keep a small time step, elevate the computational cost of the simulations.

In order to circumvent the aforementioned problems associated with conventional CFD methodologies to deal with moving boundary problem, we make use of Immersed Boundary Method (IBM) to solve the Navier–Stokes equations. In IBM, the governing discretized differential equations are solved in a Cartesian grid irrespective of the shape of the body. While simulating moving boundaries, movement of the body takes place within the fixed Cartesian grid, which means that the transient re-meshing of the fluid domain is not necessary. These advantages make the IBM an ideal method for simulating fluid flow past moving and elastically deforming boundaries. However, since the grid generated over the body is not body-fitted, enforcing the no-slip boundary condition on the surface of the body is not straightforward. Explained below are some additional steps that are necessary to incorporate the boundary conditions exactly over the body.

Among many variants of existing IBMs, we chose to use the idea of implicit force calculation [15]. Implicit calculation of Lagrangian forces eliminates the time step restriction imposed upon the computation. We make two essential changes: first, time integration of the Navier–Stokes equations have been carried out by means of a second order projection method [16], which provides second order convergence for pressure; second, we make use of the 4-point regularized delta function [17], which posses much wider stability region and results in efficient enforcement of boundary conditions than any other delta functions.

- Solve momentum equations without considering the presence of immersed boundaries and obtain intermediate velocity components $u^*(x)$. On the domain boundaries, the required boundary conditions for the problem considered are applied.

$$\frac{u^* - u^n}{\Delta t} = -\frac{3}{2}\nabla_h(uu)^n + \frac{1}{2}\nabla_h(uu)^{n-1} - \nabla_h p^n + \frac{1}{2Re}\nabla_h^2(u^* + u^n) \tag{1}$$

The convective and diffusive terms are discretized using Adams–Bashforth and Crank-Nicolson schemes respectively, which provide overall second order accuracy.

- Obtain the velocity components on the Lagrangian points $U^*(X_k)$ by interpolating nearby Eulerian points' velocities $u^*(x)$

$$U^*(X_k) = \sum_x u^*(x)\delta_h(x - X_k)h^2 \tag{2}$$

Calculate the Lagrangian forces $F^*(X_k)$ from prescribed boundary velocities $U^{n+1}(X_k)$ and interpolated velocities at Lagrangian points $U^*(X_k)$

$$\sum_{j=1}^{M}\left[\sum_x \delta_h(x - X_j)\delta_h(x - X_k)\Delta s h^2\right]F^*(X_j) = \frac{U^{n+1}(X_k) - U^*(X_k)}{\Delta t} \tag{3}$$

- Distribute Lagrangian forces $F^*(X_k)$ to the nearby Eulerian points $f^*(x)$

$$f^*(x) = \sum_{k=1}^{M} F^*(X_k)\delta_h(x - X_k)\Delta s \tag{4}$$

where Δs is the distance between adjacent Lagrangian points

- Correct the intermediate velocity $u^*(x)$ using the Eulerian forces $f^*(x)$ and obtain another intermediate velocity $u^{**}(x)$

$$\frac{u^{**} - u^*}{\Delta t} = f^* \tag{5}$$

- Solve a Poisson equation for pressure correction

$$\nabla_h^2 p' = \frac{\nabla_h \cdot u^{**}}{\Delta t} \tag{6}$$

The algebraic system of equations resulting from discretization of Poisson equation is solved using BiCGSTAB(2) algorithm [18].

- Correct pressure and velocities

$$p^{n+1} = p^n + p' - \frac{1}{2Re}\nabla_h \cdot u^{**} \tag{7}$$

$$\frac{u^{n+1} - u^{**}}{\Delta t} = -\nabla_h p' \tag{8}$$

In the above formulations, ∇_h refers to discrete gradient operator, and δ_h is the discrete Dirac delta function, which is employed to transfer the quantities between Eulerian and Lagrangian domains effectively.

For spatial differencing of momentum equations, second order central differencing is used for viscous terms. Since the upwind schemes exhibit excessive artificial diffusion characteristics, convective terms in conservative form are discretized using second order central differencing. First order Euler integration has been applied for time stepping.

The two dimensional discrete version of delta function is,

$$\delta_h(x) = \frac{1}{h^2}\phi(x)\phi(y) \tag{9}$$

where h is the Eulerian mesh width, x and y are the Cartesian components. ϕ is the hat function, which can be formulated in many ways depending upon the number of nearby points it uses. In our solver, we use 4-point delta function which ensures more accurate boundary condition imposition [17].

$$\phi(r) = \begin{cases} \frac{1}{8}(3 - 2|r| + \sqrt{1 + 4|r| - 4r^2}) & \text{if } 0 \leqslant r \leqslant 1 \\ \frac{1}{8}(5 - 2|r| + \sqrt{-7 + 12|r| - 4r^2}) & \text{if } 1 \leqslant r \leqslant 2 \\ 0 & \text{otherwise} \end{cases} \tag{10}$$

The developed solver is validated by simulating standard test cases such as flow past a stationary cylinder, steady rotating cylinder, transversely oscillating cylinder and an in-line oscillating cylinder in still fluid. The agreement of our results with those reported in the literature is excellent [19]. Furthermore, the solver has been extensively validated to simulate unsteady aerodynamics of insect flight [20,21]. The capability of our solver, in the context of present problem, is demonstrated by simulating flow past a cylinder with fixed splitter plate, the results of which are reported in the next section.

4. Flow with fixed splitter plate

Before simulating the flow past an oscillating splitter plate, the circular cylinder with fixed splitter plate is simulated at *Re* of 100 and 160. These simulations are used to validate the performance of the solver in context of the problem under consideration. For all cases with the splitter plate, the computational domain occupies $-15D \leqslant x \leqslant 40D$ and $-15D \leqslant y \leqslant 15D$ and the circular cylinder is located at the origin. This domain size is found to be sufficient enough for the vortices to get convected out of the domain without affecting the flow inside the domain. The computational domain is discretized with 454 and 271 Eulerian points respectively in *x*- and *y*-directions. The total number of Lagrangian points used to discretize the cylinder and the splitter plate together is 257. The grid independence study suggests that the number of Eulerian and Lagrangian points used is sufficient enough to capture the fluid flow accurately. A portion of non-body confirming Cartesian grid near the cylinder is shown in Fig. 2. Dirichlet and Neumann boundary conditions for velocities are applied on the inlet and outlet of the domain respectively. At the top and bottom boundaries, symmetry boundary condition is applied. The boundary conditions are schematically shown in Fig. 3.

The time averaged streamline pattern for two different *Re* are shown in Fig. 4. The comparison of characteristic quantities like drag coefficient, Strouhal number and length of the recirculation bubble (B_s) is presented in Table 1. As can be seen from the table, the computed quantities are in close agreement within the range reported in the literatures. However, the *St* and B_s have been marginally over-predicted by our simulations. This may be because of the difference in the way the Navier–Stokes equations are solved. The literatures [9,10,22] used conventional body-fitted grid solver, whereas we use Cartesian grid to discretize the computational domain. Except for marginal over-predictions, the results from the code are in good agreement with those reported by other researchers.

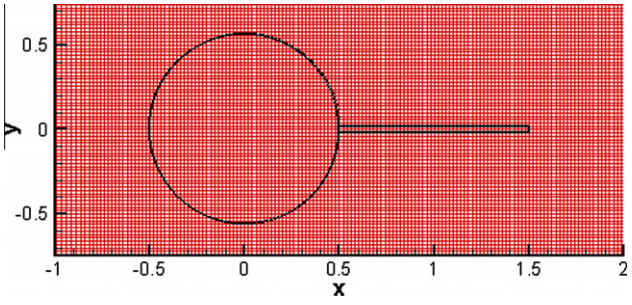

Fig. 2. Close up view of the Cartesian grid around the cylinder fitted with a splitter plate.

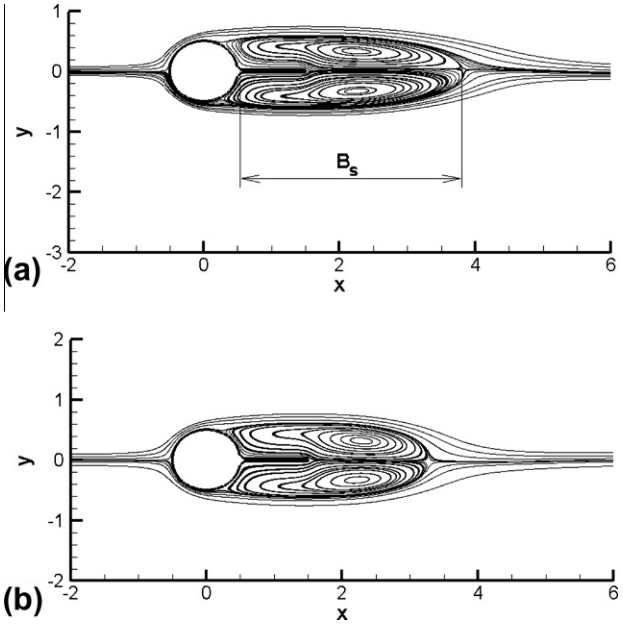

Fig. 4. Time averaged streamline patterns over the cylinder with fixed splitter plate (a) *Re* = 100 (b) *Re* = 160. Length of recirculation bubble is defined in (a).

The addition of splitter plate stabilizes the shear layers forming over the cylinder, and hence suppresses the vortex shedding. This can be observed by comparing the *St* obtained from simulation cases with- and without-splitter plate simulations at *Re* = 100 (Table 1)—the addition of splitter plate resulted in reduced frequency of shedding. In addition, the drag coefficient is also reduced from 1.37 to 1.039 due to the inclusion of wake splitter plate. However, length of the recirculation bubble is increased. All these results are consistent with those reported previously in literature.

5. Flow with oscillating splitter plate

It is well known that when *Re* of the flow exceeds 47, alternate shedding of vortices from the surface of the cylinder is observed, which is known as von-Karman vortex shedding. At the base of the cylinder, we attach a rigid splitter plate which is forced to

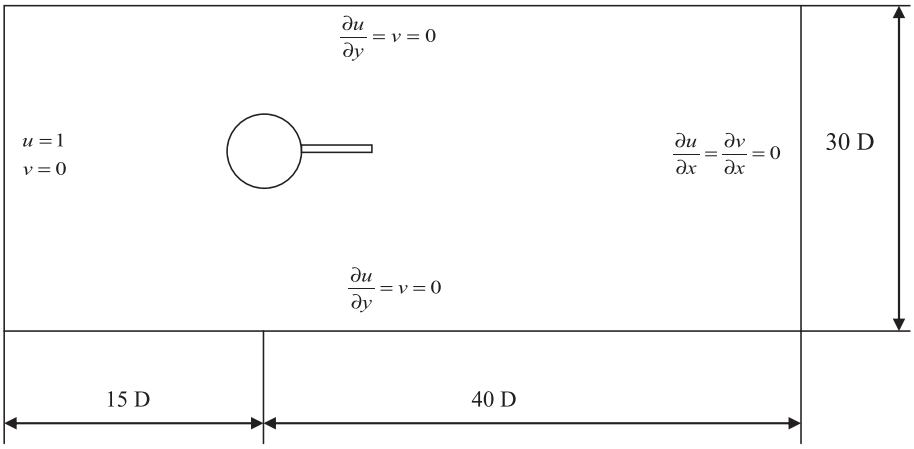

Fig. 3. Domain size and the boundary condition for the simulations.

Table 1
Comparison of characteristic quantities for flow past a circular cylinder with and without splitter plates.

Test cases		References			Present
		Hwang et al. [10]	Park et al. [22]	Kwon and Choi [9]	
Without splitter plate Re = 100	C_D	1.34	1.33	–	1.37
	St	0.167	0.164	–	0.165
	B_s	1.36	1.37	–	1.42
With splitter plate L/D = 1, Re = 100	C_D	1.17	–	1.18	1.174
	St	0.137	–	0.137	0.139
	B_s	3.21	–	3.21	3.3
With splitter plate L/D = 1, Re = 160	C_D	1.08	–	1.10	1.095
	St	0.156	–	0.155	0.159
	B_s	2.75	–	2.74	2.76

exhibit simple harmonic motion (Fig. 1). When the splitter plate starts moving, vortices are developed and shed from the tip of the plate. These shed vortices roll up to form the starting vortex from the plate. The starting vortex from the plate and the cylinder vortices are shown in Fig. 5. The most striking feature of the problem under consideration is the interaction between the starting vortex formed from the splitter plate and the vortices shed from the cylinder which form von-Karman shedding.

In order to demonstrate the nature of this phenomenon, consider a simulation case in which $A = 0.2$ and $f_s = 0.5$. The instantaneous vorticity plots, when the splitter plate is moving downward, are shown in Fig. 6. Starting vortex formed from the tip of the plate can be clearly seen in Fig. 6a. At this instance, the starting vortex interacts with the cylinder vortex which has the opposite sense of rotation. When the plate moves further downwards, the starting vortex grows in size (Fig. 6b). When the plate reaches its lowest position, the starting vortex joins with the cylinder vortex which has same sense of rotation (Fig. 6c). The consequences of such interactions (between the starting vortex and the cylinder vortices) on the flow structure and the force production are studied in-detail for different amplitudes and frequencies of oscillation. It is to be noted that when the plate moves from its highest position, the starting vortex interacts with the topside vortex from the cylinder; but when the plate reaches its lowest position, the same starting vortex merges with the bottomside vortex from the cylinder.

Since the plate moves according to a simple harmonic function, $y = A\sin(2\pi f_s t)$ the velocity of the splitter plate is maximum when it is at its mean position (horizontal). This implies that when the plate moves from outermost (either highest or lowest) position towards mean position, it is accelerated; the plate is decelerated when it moves from its mean position towards outermost position. Fig. 7a shows the plate in its mean position while moving downwards. The tip starting vortex and the shear layers formed over the bottom surface of the plate are shown in the figure. When the plate moves downwards from its mean position, it is decelerated as explained above. As a result of deceleration, we can observe that the size of the starting vortex is reduced (Fig. 7b and c). Moreover, the shear layers formed on the bottom surface of the plate moves towards the plate tip. At the same time, on the upper surface of the plate a new shear layer is formed. Upon the reversal, the tip vortex joins and merges with the cylinder vortex which is of the same sign (Fig. 7c and d). The shear layers, which were moving towards the tip of the plate, accumulate to form the starting vortex during the subsequent upward motion. It can be seen that when the plate starts moving upwards from its lowest position, the starting vortex increases in its size (Fig. 7e and f). The shear layers forming on the top surface of the plate increase in size due to this accelerated motion.

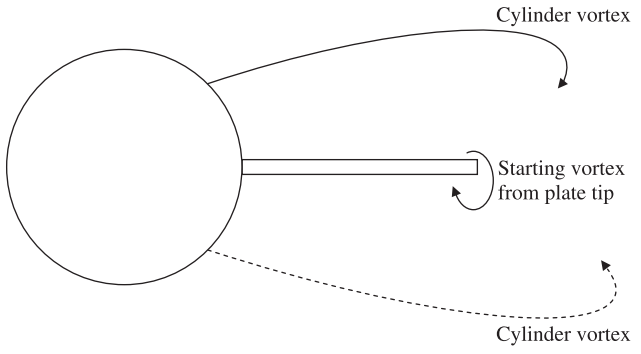

Fig. 5. Sketch showing major features of the problem under consideration. Continuous line denotes clockwise vortex and dotted line denotes anticlockwise vortex.

5.1. Vortex shedding patterns

The frequency of oscillation and the amplitude of the splitter plate significantly affect the starting vortex formed over the plate. These starting vortices interact with the vortices formed from the surface of the cylinder and leads to different patterns of vortex shedding, which can be classified into three groups as explained below. The occurrence of these different shedding patterns at different combinations of amplitude and oscillating frequency are shown in Fig. 8.

5.1.1. Normal vortex shedding

In this mode of shedding, the wake vortices qualitatively resemble the von-Karman vortex shedding from the cylinder at this Re (Fig. 9a). A single vortex is formed on the top and on the bottom side of the cylinder. They are opposite in the sense of their rotation to each other. These vortices interact to induce periodic vortex shedding from the cylinder. The starting vortices from the tip of the plate and the shear layers formed on the surface of the cylinder are not having sufficient strength to induce a complete change in the behavior of vortex shedding.

5.1.2. Chain of vortices

For certain combinations of frequency and amplitude, this distinct pattern of shedding is observed. Instead of a single vortex on the top and bottom side, chains of vortices are formed (Fig. 9b). These vortices do not initiate alternate shedding until very large distance downstream of the cylinder, after which the regular vortex shedding occurs (Fig. 10).

5.1.3. Shedding from plate

Very near to the surface of the cylinder, the wake contains alternate vortices similar to that of the normal vortex shedding (Fig. 9c). These vortices are shed from the splitter plate oscillation rather

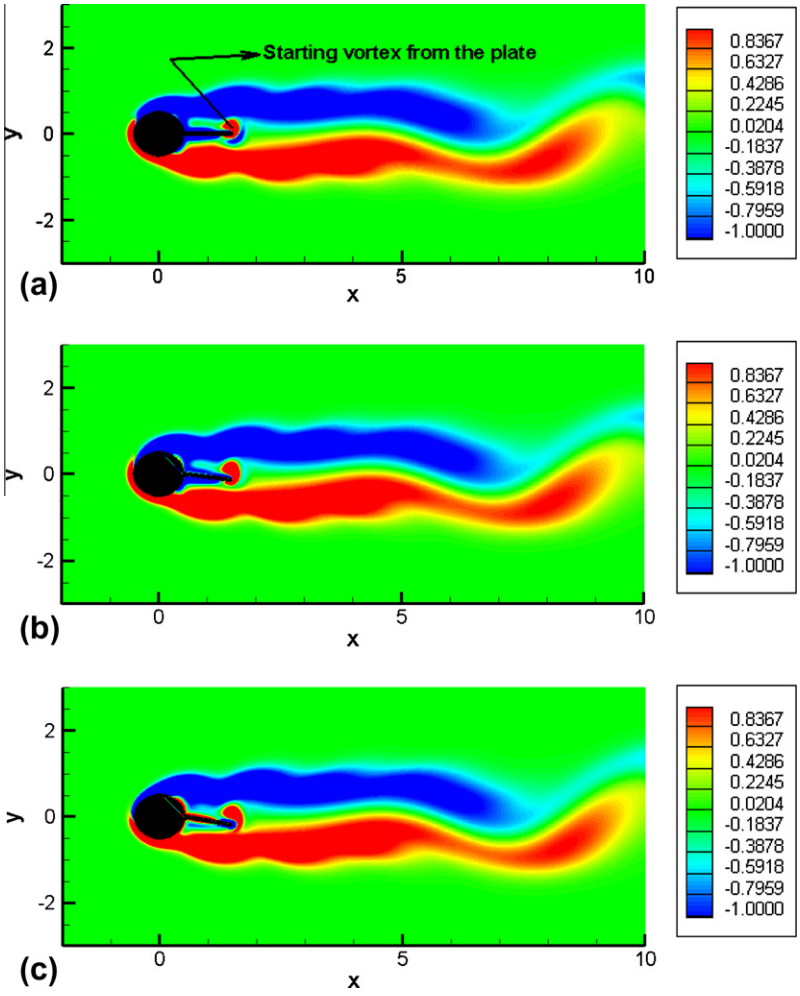

Fig. 6. Instantaneous gray scale plot of vorticity showing the interaction of starting vortex and the shed vortex from cylinder when the plate is moving downwards $A = 0.2$ and $f_s = 0.5$. The plate is at its (a) mean position showing the starting vortex (b) mid-point between mean and lowest position showing the growth of starting vortex (c) lowest position showing that starting vortex has joined with the cylinder vortex.

than from the surface of the cylinder. However, further downstream the vortical pattern is similar to that of chain of vortices.

The amplitude and frequency of splitter plate flapping and the corresponding occurrence of different patterns of vortex shedding are shown in Fig. 8. When both A and f_s are small, the vortex shedding is similar to the shedding behind a plain cylinder. In such cases, the oscillation velocity of the plate is small, so that the starting vortices shed from the splitter plate are weak. These vortices, though affect the St and C_D of Karman shedding (explained in next sections), are not capable to induce a complete change in the behavior of vortex shedding. Hence, the shedding pattern qualitatively resembles the usual von-Karman vortex shedding from the cylinder (Fig. 9a).

When the amplitude and frequency are increased, we find a distinct vortex shedding behavior. At the top and bottom side of the cylinder, instead of a single vortex, a chain of vortices is formed. It can be observed from Fig. 9b that when the top vortex is bulgy, the corresponding bottom side vortex at the same streamwise location is very thin. This implies that though the shedding pattern is qualitatively different, the vortices are separated alternatively from the cylinder surface similar to the normal shedding pattern. In a study of passive flow control using a control cylinder [24], the authors have also reported that the upper vorticity layer rolls up into several eddies of same vorticity sign having some separation distance. The vortical pattern in this case is similar to the one reported therein, but with the difference is that in our case, the separation distance (as defined in [24]) between the vortices is zero. The normal Karman shedding starts in the wake at a downstream distance of around 15 diameters, as can be seen in Fig. 10.

When both the amplitude and the frequency of flapping are very high, the starting vortex developed and shed from the tip of the splitter plate dominates the near wake of the cylinder (Fig. 9c). The vortices which are shed from the plate are very strong. Moreover, since the plate moves up to $A = 0.5D$, it disturbs the cylinder vortices to a large extent. The vortices shed from the cylinder have been obstructed when the plate is in its outermost position. Instantaneous contours of vorticity when the plate is in its highest position for different stroke amplitudes are shown in Fig. 11. When $A = 0.1$, the plate moves very small distance upwards and the starting vortex developed from the plate is of lower strength (Fig. 11a). The plate does not even make a physical contact with the vortices generated from the cylinder. When $A = 0.3$, the plate physically interferes with the vortices generated from the plate (Fig. 11b). However the wake is dominated by the cylinder vortices. When the plate oscillates with $A = 0.5D$, the starting vortex from the plate occupies the whole transverse width of the wake (Fig. 11c). In doing so, if the freestream flow is dominant, the vortex shed from the cylinder should be convected in the flow direction. But, since the starting vortex is of higher strength, the vortex which is shed from the cylinder is prohibited to move

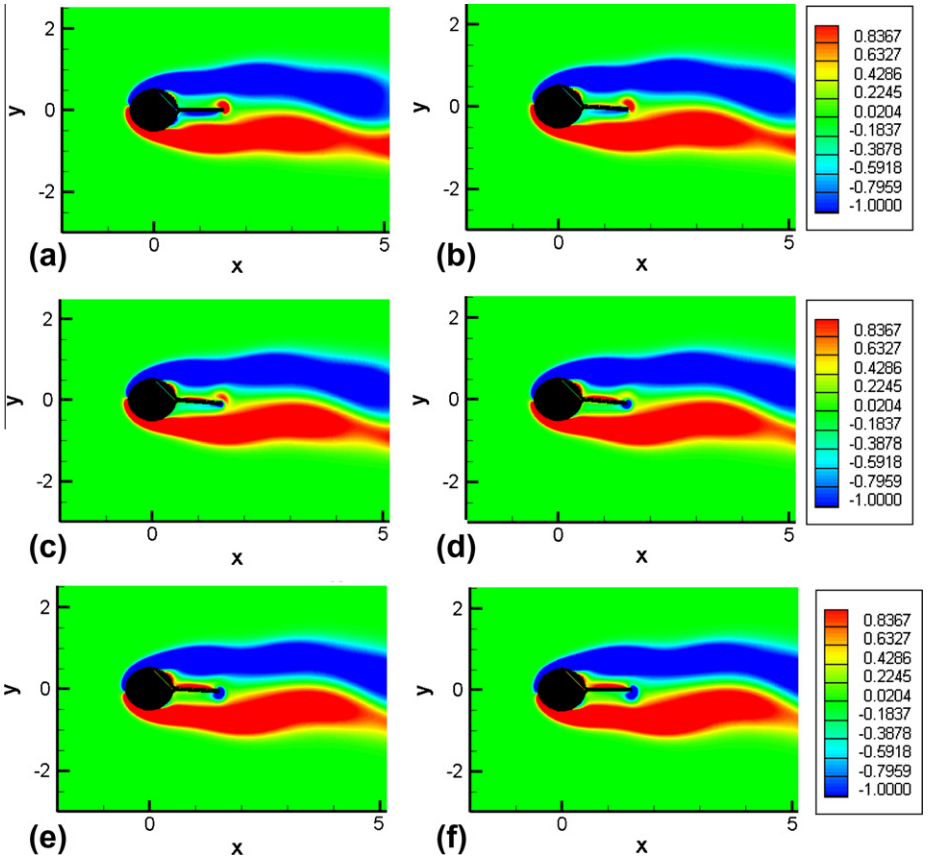

Fig. 7. Instantaneous gray scale plot of vorticity at different instances of time when $A = 0.1$ and $f_s = 0.3$.

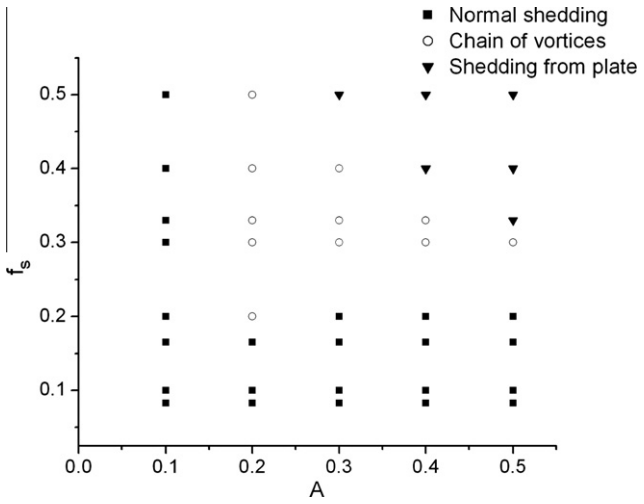

Fig. 8. Vortex shedding patterns at different splitter plate oscillation amplitudes and frequencies.

downstream. Hence it starts to stay attached to the splitter plate. During the subsequent downward movement of the plate, this cylinder vortex sheds from the plate as the starting vortex (see the starting vortex in Fig. 9c). As will be explained in the following subsection, it can be observed that for such kind of vortex shedding, the *St* is equal to the frequency of the plate oscillation. Further downstream in the wake, the vortical structure is similar to the chain of vortices (Fig. 9c).

In normal vortex shedding, the von-Karman shedding starts directly from the cylinder. As the name indicates, in chain of vortices, the von-Karman shedding starts after a chain of vortices that extends from the cylinder surface. In the third case, shedding from the plate, the near downstream wake is dominated by the starting vortices from the splitter plate. Further downstream, chain of vortices is observed, and finally ends up in von-Karman shedding.

5.2. Strouhal number

The power spectra of velocity data acquired at a point located 10D downstream on the center of cylinder is computed to find the Strouhal number (*St*). Influence on the *St* by the oscillating splitter plate is given in Table 2. The values inside the bracket represent second dominant shedding frequency.

At small frequencies of splitter plate (f_s), the *St* equals to that of f_s. Since the splitter plate is attached at the base of the cylinder, though there are two different vortex shedding characteristics (one from splitter plate and another from cylinder), the flow over the cylinder adjusts itself automatically in such a way that the shedding frequency of cylinder synchronizes with the forced frequency of splitter plate (f_s). Both the cylinder and the splitter plate act as a single system.

If f_s is increased, the *St* variation is dependent on the amplitude of splitter plate oscillation.

- At lower value of *A* (=0.1, 0.2 and 0.3), when f_s is increased, the *St* takes an intermediate value between the natural shedding frequency of the cylinder at this *Re*, which is 0.165, and the forced oscillation frequency of the splitter plate. This phenomenon can be explained as follows. When f_s is increased, the velocity of oscillation of the plate is increased when compared to low f_s case. As a result, the starting vortices shed from the tip of the plate do not have sufficient time to get convected into the wake.

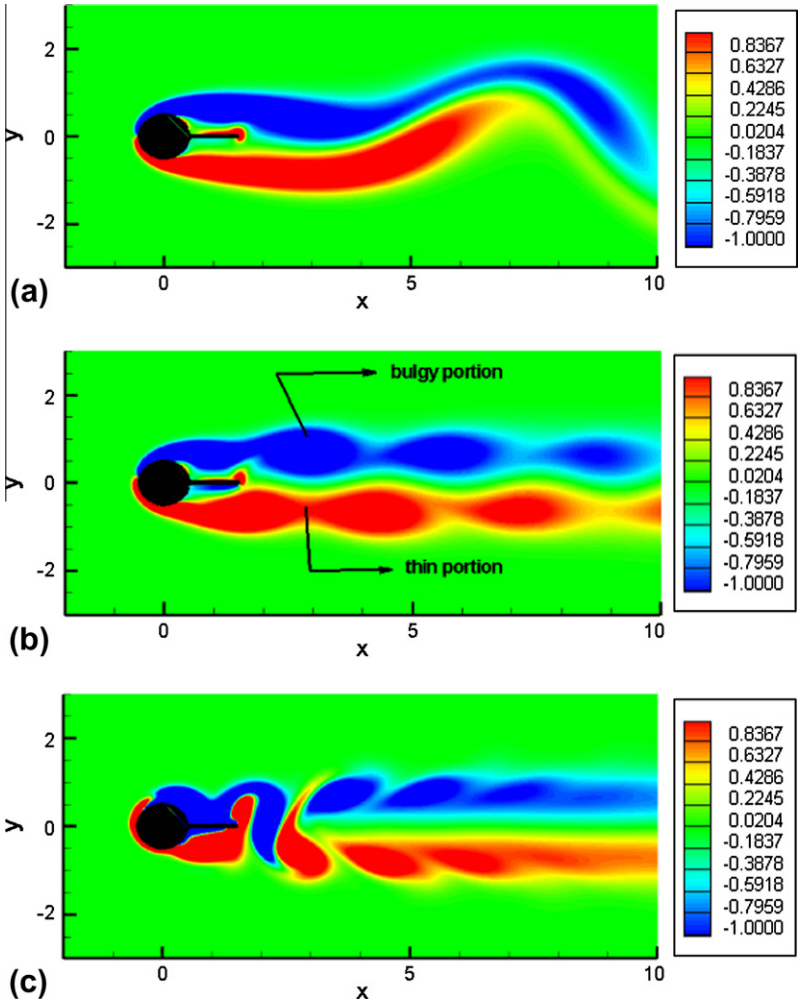

Fig. 9. Instantaneous gray scale plot of vorticity at time when the wing reached its mean position while moving downwards (a) normal vortex shedding pattern $A = 0.1$ and $f_s = 0.1$ (b) chain of vortices $A = 0.2$ and $f_s = 0.2$ (c) shedding from plate $A = 0.5$ and $f_s = 0.4$.

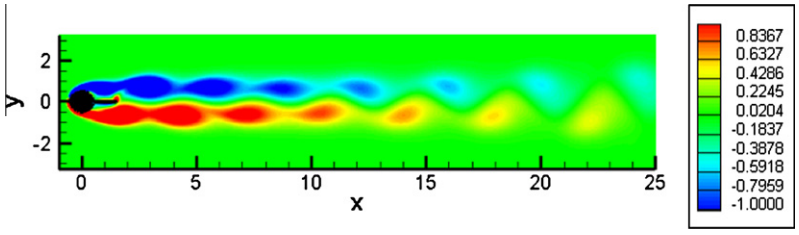

Fig. 10. Full streamwise view of Fig. 9b showing the shedding of vortices after large downstream distance.

The starting vortex shed from the plate when it was moving downward, interact with the plate when it was performing the subsequent upward travel due to the inadequate convective velocity. Hence the *St* of the system is changed from f_s.

- At higher value of *A*, the wake dynamics is dominated by the starting vortices shed from the splitter plate, and hence *St* becomes equal to f_s. Moreover, since the plate moves to a larger distance, the vortices are convected into the wake before the plate returns on its path in the subsequent motion. Hence the vortex-plate interaction described for lower *A* cases are not observed here.

In between these two cases, both the cylinder vortices and the starting vortices from the plate interact in a complex manner, to give rise to multiple vortex shedding frequencies (Fig. 12).

When *A* is increased keeping f_s as constant, the strength of the vortices shed from the splitter plate is increased, owing to the increasing velocity with which the plate travels at higher A. However, as explained above, since the flow adjusts itself to match with the splitter plate frequency, the *St* is not changed when *A* is increased (see Table 2 for $f_s = 0.165$ at different values of *A*). The power spectra of velocity for $f_s = 0.165$, shown in Fig. 13 for different amplitudes, indicate that though the frequency is not changed, the increased strength of starting vortices manifests in increased power at higher *A*. This implies that at higher *A*, the cylinder sheds strong vortices in the wake at the same frequency.

This amplitude independency is in contrast to the results reported for another flow control strategy – control cylinder in the wake [26]. A small control cylinder was placed in the wake of the main cylinder at different points within the recirculation

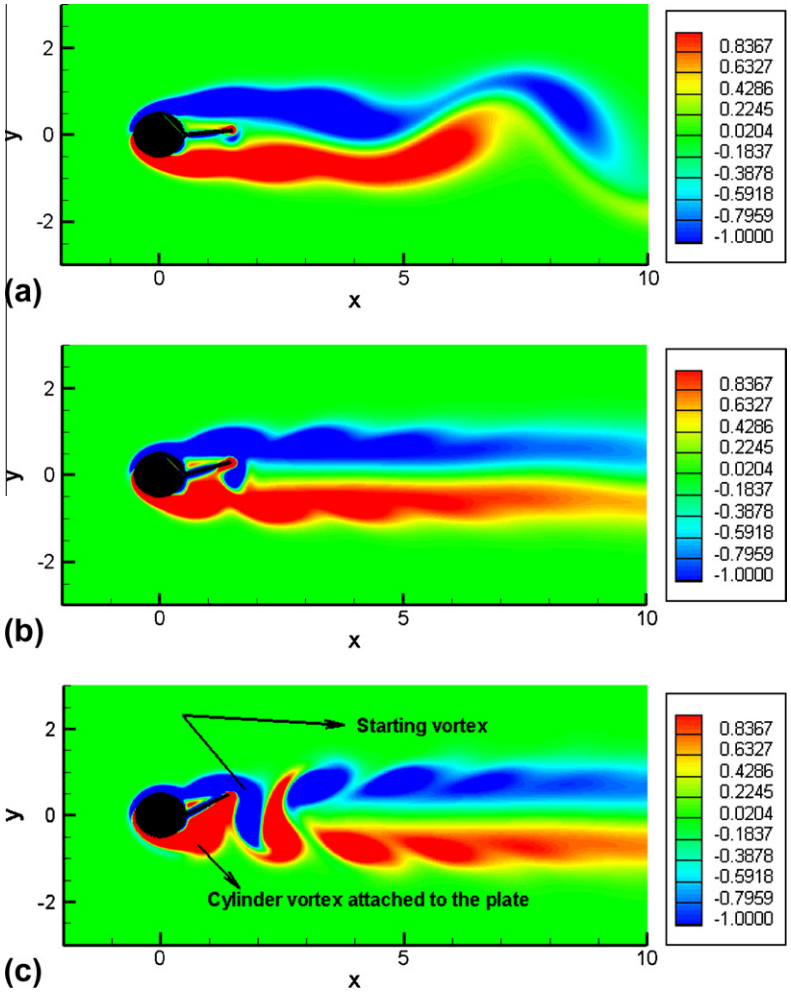

Fig. 11. Instantaneous gray scale plot of vorticity at time when the plate reached its highest position (a) $A = 0.1$ $f_s = 0.4$ (b) $A = 0.3$ $f_s = 0.4$ (c) $A = 0.5$ $f_s = 0.4$.

Table 2
Strouhal number for different amplitude and oscillation frequencies.

f_s	A				
	0.1	0.2	0.3	0.4	0.5
0.0825	0.14 (0.0825)	0.0825	0.0825	0.0825	0.0825
0.1	0.1	0.1	0.1	0.1	0.1
0.165	0.165	0.165	0.165	0.165	0.165
0.2	0.133 (0.2)	0.2 (0.128)	0.2	0.2	0.2
0.3	0.14	0.14	0.3 (0.126)	0.3	0.3
0.33	0.138	0.138	0.33 (0.138)	0.33	0.33
0.4	0.138	0.138	0.148 (0.4)	0.4 (0.148)	0.4 (0.138)
0.5	0.135	0.135	0.148 (0.5)	0.247 (0.5)	0.5 (0.125)

region. Any perturbation created at any point in the recirculation zone resulted in a change of global frequency. This was attributed to the interaction between the shear layers formed over the main cylinder and that of control cylinder. As reported in the previous sections, such kind of vorticity interactions occurs in our simulations also. Though the change in amplitude of splitter plate oscillation results in a change in the strength of tip vortex generated from the plate, which in turn induces a perturbation in the wake, the global frequency is not altered in present simulations. The following facts are mainly responsible for the observed difference between the control cylinder and splitter plate flow physics.

- The control cylinder was placed at different points in the wake of the main cylinder, where the wake velocity is different. Due to this, the free stream flow experienced by the control cylinder was changed, and hence the frequency of vortex shedding from the control cylinder. This difference in the shedding frequency

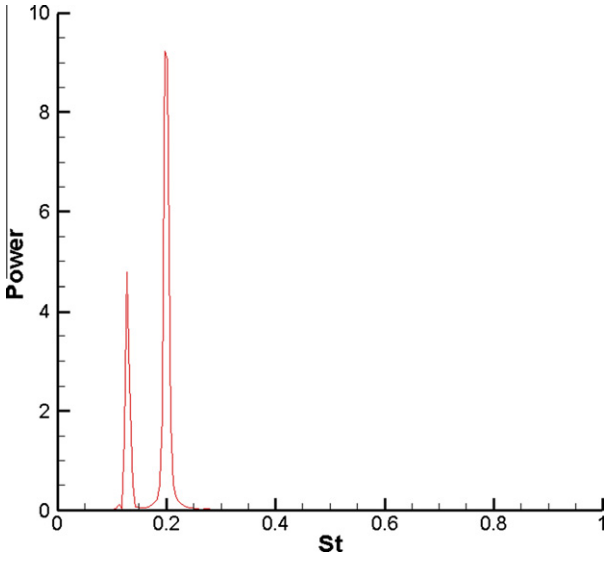

Fig. 12. Power spectral density of velocity signal at a point 10D downstream of the cylinder center for $A = 0.2$ and $f_s = 0.2$.

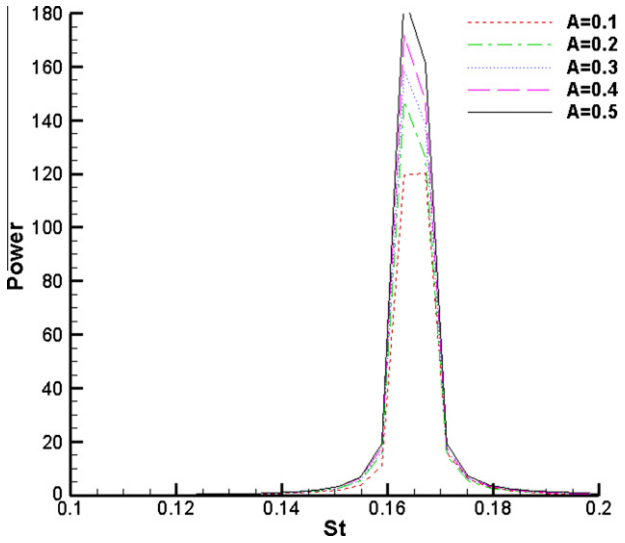

Fig. 13. Power spectral density of velocity signal at a point 10D downstream of the cylinder center for different amplitudes at $f_s = 0.165$.

of control cylinder resulted in the change in global frequency. In the present case, the splitter plate is forced to oscillate at the desired frequency. Even when amplitude of splitter plate is varied, the strength of vortices formed over the plate is changed, but the frequency of shedding remains unchanged.

- The nature of interaction between the main and control cylinder was changed when the position of control cylinder was changed. Whereas, in present simulations, always the tip vortex from the splitter plate during its downward movement interacts with the shear layers formed on the downside of the cylinder and vice versa.
- In present simulations, the splitter plate vortices and main cylinder vortices develop simultaneously, and interact with each other before they are convected into the wake and starts forming von-Karman shedding. In control cylinder experiments, the shedding from the cylinder develops first, which interact with the von-Karman shedding from the control cylinder.

The experiments at higher *Re* (=145,000) [2] as well the numerical simulations at low *Re* (=160) [9] have shown that in order to completely suppress the vortex shedding from a circular cylinder, a splitter plate of length equivalent to 5 times the diameter of the cylinder ($L/D = 5$) is required. It can be seen from Table 1 that when a fixed splitter plate of $L/D = 1$ is attached to the cylinder, the *St* is decreased from 0.165 (without splitter plate) to 0.139. Though *St* is reduced, the reduction is not highly significant. However, present simulations with oscillating splitter plate at $f_s = 0.0825$ has shown that for the same $L/D = 1$, the *St* is reduced to 0.0825 (Table 2). This leads to the conclusion that a short splitter plate itself is capable of suppressing the vortex shedding frequencies from bluff bodies to a large extent, when the plate is given simple harmonic oscillation at very low oscillating frequencies.

Gerrard [3], from his experiments on fixed splitter plate, has suggested that the frequency of von-Karman vortex shedding is inversely proportional to the vortex formation length (l_f) immediately downstream of the bluff body. Such a conclusion is found to be true for the splitter plate attached to a freely rotatable cylinder also [7]. However, such an inverse relationship between the vortex formation length and the Strouhal number is not valid when the splitter plate is subjected to perform forced oscillation. We follow the same definition used in [6] to define l_f (Refer Fig. 1 in [6]).

Table 3
Vortex formation length (l_f) for different amplitude and oscillation frequencies.

f_s	A				
	0.1	0.2	0.3	0.4	0.5
0.0825	1.624	1.626	2.909	2.937	2.955
0.1	1.628	1.626	2.33	2.402	2.466
0.165	2.124	2.22	2.143	2.108	2.057
0.2	1.788	12.08	1.781	1.746	1.715
0.3	1.624	5.66	22.176	19.828	27.648
0.33	1.626	5.183	15.868	26.681	25.885
0.4	1.629	4.371	16.361	29.60	26.43
0.5	1.628	4.20	12.722	26.162	18.782

By comparing the *St* given in Table 2, and l_f given in Table 3, we can observe that no such relationship exists in our simulation of oscillating splitter plate case.

Simulations of Kwon and Choi [9] showed that due to the appearance of the secondary vortex on the tip of the plate, which is of opposite in the sense of its rotation to the primary vortex, the *St* was found to increase. However, in our simulations the tip vortex which is analogous to the secondary vortex of their simulations is present in all the cases. If the appearance of this tip vortex can increase the *St*, the *St* produced in our cases should be higher than that of produced over a stationary splitter plate at this *Re*, where there is no secondary vortex. But contrary to this, the *St* with stationary splitter plate at $Re = 100$ (Table 1) is higher than many of our simulations (Table 2) where the tip vortex is present. This observation is contrary to the results reported in [6] for stationary splitter plate. This may be because of the fact that in our simulations the tip vortex is forced to form at a pre-defined frequency, in contrast to [6], in which the tip vortex is free to form on its own.

5.3. Drag coefficient

The averaged drag coefficient (C_D) for different oscillation frequencies and amplitudes are given in Table 4. It is seen that when the frequency is increased from 0.0825 to 0.165, C_D increases gradually. In all the amplitudes considered, except for $A = 0.5$, C_D is maximum when $f_s = 0.165$. When there is no splitter plate attached to the circular cylinder, the natural vortex shedding occurs at $St = 0.165$ (Table 1). This coincidence is surprising. It could be because of the fact that since the *St* of plain cylinder and the splitter plate frequency are the same, the vortices shed from the plate reinforces the shedding from the cylinder. Hence C_D is increased. When f_s is increased beyond 0.165, the variation of C_D is different for different amplitudes (Fig. 14). At low amplitudes ($A = 0.1, 0.2$) C_D decreases when f_s is increased from 0.165 to 0.2, and does not vary greatly when f_s is further increased. When $A = 0.3$ and 0.4, C_D decreases rapidly, when f_s is increased from 0.165 to 0.3. In contrary to the low amplitude cases, when f_s is further increased, C_D decreases gradually. The highest amplitude considered ($A = 0.5$)

Table 4
Coefficient of drag for different amplitude and oscillation frequencies.

f_s	A				
	0.1	0.2	0.3	0.4	0.5
0.0825	1.167	1.1699	1.181	1.1765	1.1706
0.1	1.185	1.235	1.2626	1.2731	1.286
0.165	1.2567	1.308	1.3442	1.367	1.3895
0.2	1.166	1.136	1.309	1.357	1.4398
0.3	1.169	1.153	1.135	1.151	1.178
0.33	1.168	1.148	1.1245	1.135	1.1848
0.4	1.163	1.134	1.0944	1.0998	1.2108
0.5	1.151	1.109	1.0503	1.07442	1.3432

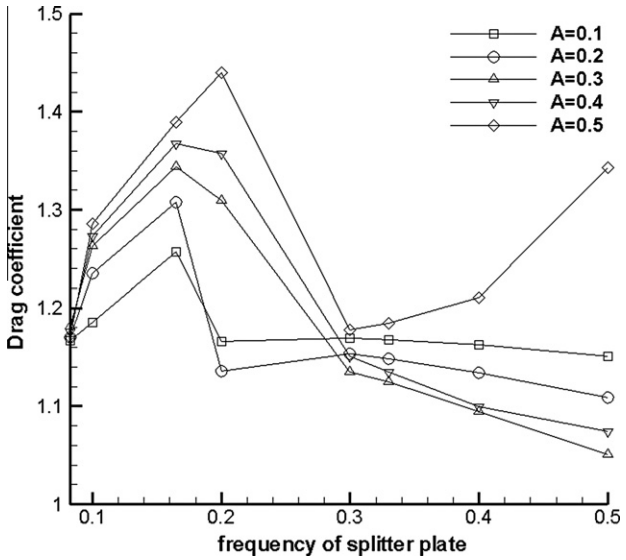

Fig. 14. Variation of coefficient of drag with frequency for different amplitudes.

shows completely different C_D vs f_s behavior. The maximum C_D occurs when $f_s = 0.2$, then C_D reduces rapidly when f_s is increased from 0.2 to 0.3. Moreover, in contrast to the other amplitudes, when f_s is further increased, C_D has also increased.

Apelt and West [4] reported that the variation of C_D follows the similar trend of *St* variation in their experiments at higher *Re* ($=5 \times 10^4$). However, recent numerical simulations over a circular cylinder attached with a fixed splitter plate [9] at $Re = 100$ predicted that such similar trends in the variation of *St* and C_D does not exist. This fact was attributed to the *Re* effect. In present simulations also, by comparing Tables 2 and 4, we did not find any similarity in the variation of C_D and *St*. Hence our simulations provide additional confidence to make a conclusion that at low *Re* laminar flow, in contrast to high *Re* turbulent flow, the variation of C_D does not follow the variation of *St*.

Previous investigations have shown that the inclusion of a fixed splitter plate at the base of a circular cylinder has increased the base pressure and resulted in the reduction of drag coefficient [2–6,9,10,23]. However, surprisingly, for some cases of amplitude and frequency combinations, the coefficient of drag presented in Table 4 is higher than the C_D of circular cylinder without splitter plate (given in Table 1). The addition of oscillating splitter plate has resulted in increased C_D. The physical basis of this drag increment can be learnt from Figs. 15 and 16. As can be seen in Fig. 15, a low pressure region is developed on the rear surface of the cylinder. Owing to the presence of the low pressure region in the rear portion of the cylinder, the pressure drag exerted over the cylinder is increased. Hence, the drag coefficient increases. It is of interest to know whether the low pressure region is the result of Karman shedding or is it because of the oscillation of splitter plate. The instantaneous pressure contours for a fixed splitter plate case presented in Fig. 16 shows no evidence of such a low pressure region. Therefore, the low pressure region is a characteristic feature associated with oscillating splitter plate. When the splitter plate is oscillated in the wake of the cylinder, the rapid movement of the plate introduces a low pressure region in the wake. This occurs in the rear portion of the cylinder and upper surface of the plate when the plate is moving downwards, as shown in Fig. 15a. When the plate exhibits upward motion, the same low pressure region occurs over the rear of the cylinder and bottom surface of the plate. When the plate is moving downwards from its mean position, the low pressure region grows in size as can be seen from Fig. 15b and c.

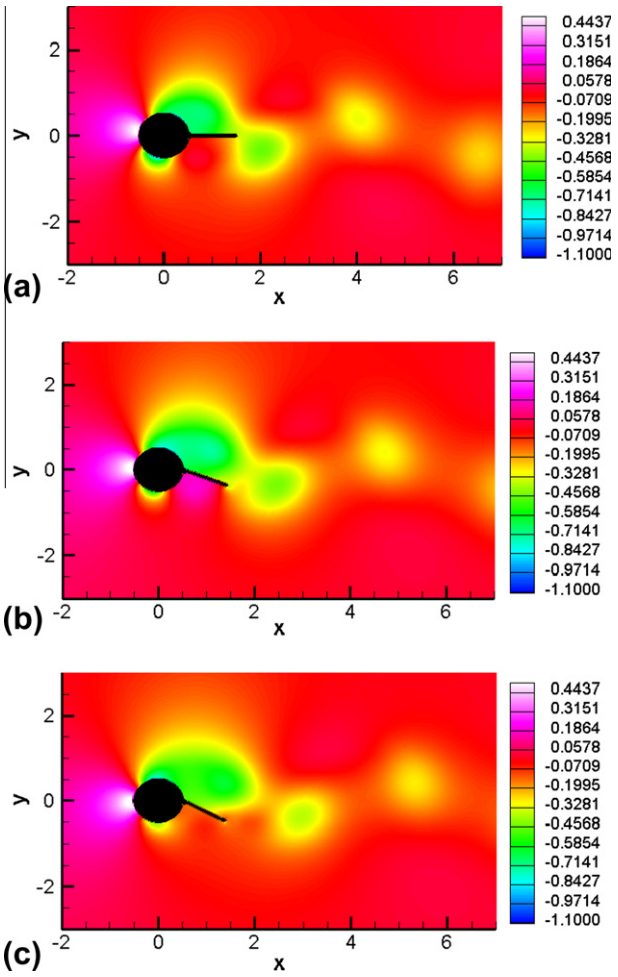

Fig. 15. Instantaneous gray scale plot of pressure when the plate is moving from its mean position to the lowest position at $A = 0.5$ and $f_s = 0.165$ (a) mean position (b) mid-way between mean and lowest position (c) lowest position.

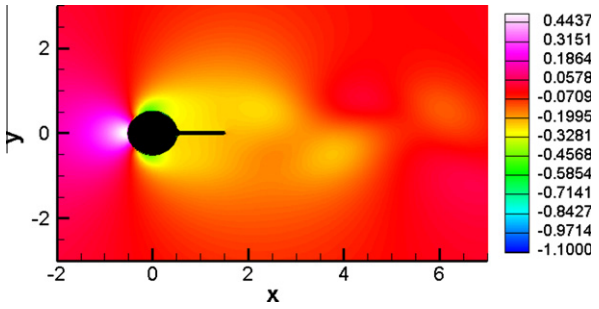

Fig. 16. Instantaneous gray scale plot of pressure for a fixed splitter plate.

Among all the simulations considered, the minimum drag coefficient $C_D = 1.0503$ occurs when $A = 0.3$ and $f_s = 0.5$. This is less than the minimum value reported for the case of the stationary splitter plate at the same *Re* with *L*/*D* of 4.5 [9]. However, the "steady" drag coefficient at $Re = 100$, reported by Fornberg [25] is 1.058. The term "steady" means that the drag coefficient obtained in the absence of any vortex shedding and splitter plate. It is interesting to note that the minimum drag value obtained in our simulations coincides with the "steady" drag value reported at the same *Re*.

As has been explained in the previous subsection, the inverse relationship between the *St* and the vortex formation length does not hold in case of oscillating splitter plate. By observing the

tabulated values of vortex formation length (Table 3) and drag coefficient (Table 4), we can conclude that there is no relationship exists between l_f and C_D. The reason for this observed difference is explained below.

In flow past a plain circular cylinder and the cylinder attached with a stationary splitter plate, when *Re* is changed, the strength of the vortices developed on the surface on the cylinder is also altered. This change in vortex strength is reflected as the change in vortex formation length and *St*. In other words, the vortices in these cases, are free to choose their shedding frequency and formation length when their strength is changed. However in present simulations at any particular frequency, when the amplitude (A) is increased, the strength of the starting vortex from the plate is increased. Because of their subsequent interaction, the strength of cylinder vortex is also altered as A is changed. Despite the change in strength of the vortices, the *St* remains constant. In contrast to the plain cylinder case, in case of flow past cylinder with oscillating splitter plate, even when the vortex strength is changed, the vortices are constrained to shed at a particular frequency. This difference is responsible for the non-applicability of Gerrard's model.

5.4. Other interesting flow features

For some combinations of amplitude and oscillating frequency, we find that the outer surface of the shear layer posses a wavy shape (Fig. 6). The reason for the existence of wavy shape is explained as follows. When an airfoil is rapidly started, a starting vortex develops behind it. The developed vortex will move away from the airfoil during the course of its motion. Similarly, in the present case, the starting vortex developed at the tip of the plate also tries to move in the direction opposite to the direction of motion of the plate (Fig. 6a and b). However, while trying to do so, it encounters the vortex shed from the cylinder, which is of opposite in the sense of its rotation. Hence, the vortex cannot move in its desired direction; but as more and more vorticity is created because of the continual movement of the splitter plate, the starting vortex increases in its size. To accommodate this increase in the size of starting vortex, the inner surface of the cylinder vortex curves towards the movement of starting vortex and as a result, the outer layer of the vortex attains a wavy shape.

During the transition period in the nature of vortex shedding from 'chain of vortices' to the 'shedding from plate', the chain vortices formed from the cylinder split. One such case is presented in Fig. 17 for the case of $A = 0.4$ and $f_s = 0.3$. When the splitter plate is moving downward, starting vortex develops from the plate which is of anticlockwise in the sense of its rotation (Fig. 17a). This starting vortex interacts with the anticlockwise vortex shed from bottom side of the cylinder. Both vortices merge into a single vortex (Fig. 17b). This single vortex interacts with the clockwise vortex developed and shed from the upper side of the cylinder. At the point of their interaction, the clockwise vortex splits into two vortices (Fig. 17c). When the amplitude is further increased, the

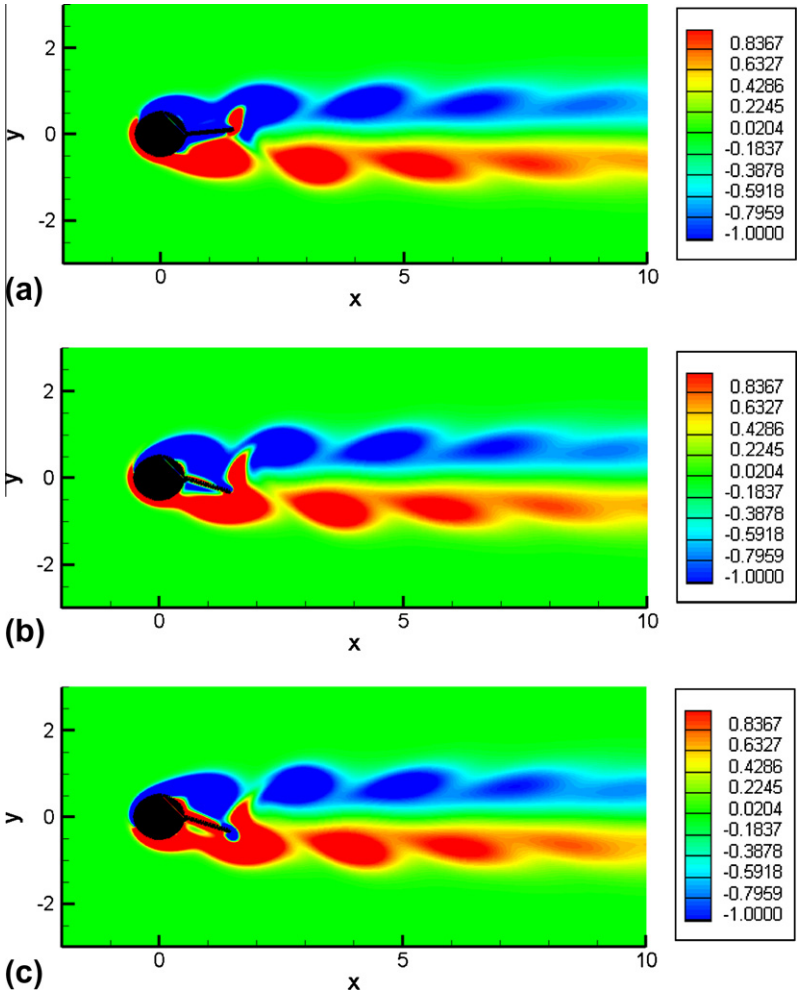

Fig. 17. Instantaneous gray scale plot of vorticity different instances of time when the plate is moving downwards $A = 0.4$, $f_s = 0.3$ (a) starting vortex formed over the plate (b) starting vortex merges with the vortex of same sign formed from the cylinder (c) vortex splitting.

starting vortex further increase in strength and the vortex pattern shifts to the shedding from plate type (Refer Fig. 9c).

6. Conclusions

The important finding from our simulations is the presence of three kinds of vortex shedding patterns which are observed at different combinations of shedding amplitude and frequency. They are normal shedding, chain of vortices and shedding from the plate. Our study also indicates that the vortex shedding can be completely suppressed by a short splitter plate ($L/D = 1$) if it is given a simple harmonic oscillation at very low oscillating frequencies. If the plate is held stationary, such a suppression requires a plate of length equivalent to five times that of the diameter of the cylinder ($L/D = 5$). Hence, in applications where space constraints limit the use of stationary splitter plate of $L/D = 5$, the shorter splitter plate with enforced oscillations can be used to suppress the vortex shedding.

References

[1] Kumar RA, Sohn CH, Gowda BHL. Passive control of vortex-induced vibrations: an overview. Rec Pat Mech Eng 2008;1:1.
[2] Roshko A. On the drag and shedding frequency of two-dimensional bluff bodies. NACA Tech Note no. 3169; 1954.
[3] Gerrard JH. The mechanics of the formation region of vortices behind bluff bodies. J Fluid Mech 1966;25:401.
[4] Apelt CJ, West GS, Szewcyyk AA. The effects of wake splitter plates on the flow past a circular cylinder in the range 10^4<Re<5 * 10^4. J Fluid Mech 1973;61:187.
[5] Unal MF, Rockwell D. On vortex formation from a cylinder. Part 1. The initial instability. J Fluid Mech 1988;190:491.
[6] Unal MF, Rockwell D. On vortex formation from a cylinder. Part 2. Control by splitter-plate interference. J Fluid Mech 1988;190:513.
[7] Cimbala JM, Garg S. Flow in the wake of a freely rotatable cylinder with splitter plate. AIAA J 1991;29:1001.
[8] Nakamura Y. Vortex shedding from bluff bodies with splitter plates. J Fluid Struct 1996;10:147.
[9] Kwon K, Choi H. Control of laminar vortex shedding behind a circular cylinder using splitter plates. Phys Fluids 1996;8:479.
[10] Hwang JH, Yang KS, Sun SH. Reduction of flow induced forces on a circular cylinder using a detached splitter plate. Phys Fluids 2003;15:2433.
[11] Celik B, Akdag U, Gunes S, Beskok A. Flow past an oscillating circular cylinder in a channel with an upstream splitter plate. Phys Fluids 2008;20:103603.
[12] Okajimja A, Nakamura A, Kosugi T, Uchida H, Tamaki R. Flow-induced in-line oscillation of a circular cylinder. Euro J Mech B/Fluids 2004;23:115.
[13] Shukla S, Govardhan RN, Arakeri JH. Flow past a cylinder with a hinged-splitter plate. J Fluid Struct 2009;25:713.
[14] Mansy H, Yang PM, Williams DR. Quantitative measurements of three-dimensional structures in the wake of a circular cylinder. J Fluid Mech 1994;270:277.
[15] Su SW, Lai MC, Lin CA. An immersed boundary technique for simulating complex flows with rigid boundary. Comput Fluids 2008;36:313.
[16] Brown DL, Cortez R, Minion ML. Accurate projection methods for the incompressible Navier-Stokes equations. J Comput Phys 2001;168:464.
[17] Shin SJ, Huang WX, Sung HJ. Assessment of regularized delta functions and feedback forcing schemes for an immersed boundary method. Int J Numer Methods Fluids 2008;45:263.
[18] Van der Vorst HA. Iterative methods for large linear systems. Tech. Report. Mathematical Institute, Utrecht University; 2000.
[19] Sudhakar Y, Vengadesan S. Computation of viscous flow past moving bodies: use of immersed boundary method. In: 10th annual AeSI CFD symposium, Bangalore, India; 2008.
[20] Sudhakar Y, Vengadesan S. The functional significance of delayed stall in insect flight. Numer Heat Transfer Part A 2010;58:65.
[21] Sudhakar Y, Vengadesan S. Flight force production by flapping insect wings in inclined stroke plane kinematics. Comput Fluids 2010;39:683.
[22] Park J, Kwon K, Choi H. Numerical solutions of flow past a circular cylinder at Reynolds numbers up to 160. KSME Int J 1998;12:1200.
[23] Anderson EA, Szewczyk AA. Effect of a splitter plate on the near wake of a circular cylinder in 2 and 3-dimensional flow configurations. Exp Fluids 1997;23:161.
[24] Thiria B, Cadot O, Beaudoin JF. Passive drag control of a blunt trailing edge cylinder. J Fluids Struct 2009;25:766.
[25] Fornberg B. A numerical study of steady viscous flow past a circular cylinder. J Fluid Mech 1980;98:819.
[26] Parezanovic V, Cadot O. The impact of local perturbation on global properties of a turbulent wake. Phys Fluids 2009;21:071701.